Communications in Physics, Vol. 24, No. 4 (2014), pp. 353-362
DOI:10.15625/0868-3166/24/4/4180

EFFECT OF Cr^{3+} CONCENTRATION AND HEAT-TREATMENT ON STRUCTURAL PROPERTY OF Cr^{3+}-DOPED TiO_2 NANOWIRES SYNTHESIZED BY HYDROTHERMAL METHOD

TRINH THI LOAN AND NGUYEN NGOC LONG
Faculty of Physics, Hanoi University of Science,
334 Nguyen Trai, Thanh Xuan, Hanoi, Vietnam

E-mail: longnn@vnu.edu.vn

Received 09 July 2014
Accepted for publication 24 October 2014

Abstract. *Anatase $Ti_{1-x}Cr_xO_2$ nanowires with Cr^{3+} dopant contents ranging from x = 0 to 0.1 have been successfully synthesized by hydrothermal method. The nanowires were prepared from anatase titanium dioxide (TiO_2) powders, chromium nitrate ($Cr(NO_3)_3$), and sodium hydroxide (NaOH). The effect of the Cr^{3+} concentration and heat-treating temperature on crystal structure, morphology and Raman spectra of the synthesized $Ti_{1-x}Cr_xO_2$ samples has been studied in detail by X-ray diffraction, scanning electron microscopy and Raman spectroscopy. The results showed that the samples heat-treated at low temperature ($\leq$600 °C) exhibited anatase phase and for Cr^{3+}-doped anatase TiO_2 samples with $x \geq 0.01$, Raman spectra showed a new series of peaks at 120, 236, 250, 292, 362, 430, 467 and 550 cm^{-1}, which were assigned to the localized vibrational modes related to the complexes containing Cr^{3+} ions. The samples heat-treated at high temperature (1100 °C) exhibited rutile phase. It was observed that the characteristic Raman modes (E_g and M) for rutile TiO_2 were shifted and broadened with increasing Cr^{3+} dopant content. This phenomenon proves that the Cr^{3+} ions have replaced the Ti^{4+} ions in the rutile TiO_2 host lattice. It was found that the lattice constants of both the rutile and anatase TiO_2 were not changed when Cr^{3+} dopant contents were varied.*

Keywords: TiO_2:Cr^{3+} nanowires, hydrothermal method, structural property.

I. INTRODUCTION

In recent years, the nanometer-sized materials have attracted considerable attention because of their unique physical and chemical properties and their important applications. Among the nanomaterials, TiO_2 is one of the most interesting. TiO_2 has been used in many areas such as photocatalysis, photocells, hydrogen storage, and chemical gas sensors, biological liquids [1–6]. The pure TiO_2 is especially active in the ultraviolet light range because of its large band gap energy. For practical applications such as photocatalysis, photovoltaic solar cells, solar energy is the most important energy source; the large band gap of the pure TiO_2 limits the use of the wide energy window of sun light. Hence, various works have been carried out to extend the response of photoactivity of TiO_2 to visible region. It was found that by doping with transition metal ions, the

activity of TiO_2 is extended to the visible light region, resulting in enhance of the photoactivity efficiency [5, 6].

There are many methods for synthesis of TiO_2 nanomaterials such as sol-gel, hydrothermal, spin-on, anodic oxidative hydrolysis, sonochemical, pyrolysis routes, etc. Of which, hydrothermal method is simple and effective to create one-dimensional TiO_2 nanostructures such as nanorods, nanotubes, nanowires and nanobelts.

In the present study, $Ti_{1-x}Cr_xO_2$ nanowires were synthesized by two-stage hydrothermal method using 10 M NaOH aqueous solution, anatase TiO_2 powders and 0.02 M $Cr(NO_3)_3$ aqueous solution as the precursors. The effect of the Cr^{3+} concentration and heat-treating temperature on structural properties, Raman spectra and morphology of the synthesized $Ti_{1-x}Cr_xO_2$ samples has been investigated in detail.

II. EXPERIMENTAL

The anatase $Ti_{1-x}Cr_xO_2$ nanowires with Cr^{3+} contents ranging from x = 0 to 0.1 have been prepared by two-stage hydrothermal method. Commercial anatase TiO_2 powders, $Cr(NO_3)_3$ aqueous solutions, and NaOH aqueous solutions were used as the starting materials for the synthesis of anatase $Ti_{1-x}Cr_xO_2$ nanowires.

The first stage: 1 g of TiO_2 was dispersed in 100 ml of 10 M solution of NaOH, followed by steady stirring for 30 min. Then, an appropriate quantity of 0.02 M solution of $Cr(NO_3)_3$ was added to the above solution, followed by continuous steady stirring. TiO_2 powders and $Cr(NO_3)_3$ solutions were mixed with mole ratios of (1-x):x. The solution was transferred into Teflon-lined steel autoclave. The autoclave then was put in a drying cabinet and kept at temperature of 200 °C for 24 h and then cooled naturally to room temperature. Thereafter, the precipitate was filtered and washed with HCl, distilled water and ethanol and dried in air at 60 °C for 5 h.

The second stage: The resulting powders of the first stage were poured back into Teflon-lined steel autoclave with 100 ml of distilled water and kept at temperature of 130 °C for 15 h. Finally, the precipitate was filtered and dried in air at 100 °C for 24 h.

The crystal structure of the samples was determined by a Siemens D5005 Bruker, Germany X-ray diffractometer (XRD) with Cu-$K_{\alpha 1}$ irradiation (λ = 1.54056 Å) . The morphology of the samples was observed by using a JEOL-JSM 5410 LV Japan scanning electron microscope. The composition of the samples was determined by an energy-dispersive X-ray (EDX) spectrometer (EDS, OXFORD ISIS 300) attached to the JEOL-JSM 5410 LV scanning electron microscope (SEM). Raman spectra were measured using LabRam HR800, Horiba spectrometer with 632.8 nm excitation.

III. RESULTS AND DISCUSSION

To study the effects of manufacturing conditions on the formation of anatase crystalline phase, the XRD patterns of the TiO_2 samples after different stages of hydrothermal process were investigated and are shown in Fig. 1. After the first stage of hydrothermal process, a very strong diffraction peak lying at 2θ = 10.8° and some very week peaks at 2θ = 22.6°, 35.7°, 46.3° and 56.4° were observed in the XRD pattern of the samples (Fig. 1 line a). All the peaks correspond well to the $H_2Ti_5O_{11}\cdot H_2O$ phase [7], in which the peak at 2θ = 10.8° corresponds to plane (200) of the $H_2Ti_5O_{11}\cdot H_2O$ phase. However, after the hydrothermal second stage at 110 °C for 15 h,

the intensity of the characteristic diffraction peaks for the $H_2Ti_5O_{11}\cdot H_2O$ phase are significantly reduced, in addition, several new peaks lying at $2\theta = 25.3°$, $37.9°$, $47.9°$, $53.9°$ and $62.7°$ appear (Fig. 1 lines b, c, d). These peaks can be indexed as (101), (004), (200), (105) and (204) diffraction planes of anatase phase of TiO_2, respectively. When the hydrothermal temperature in the second stage increases to 120 °C, the characteristic diffraction peaks for the $H_2Ti_5O_{11}\cdot H_2O$ phase are not observed. When the temperature rises to 130 °C, the samples show a pure anatase phase of TiO_2. Therefore, for the next study, all samples must experience the hydrothermal second stage at 130 °C for 15 h.

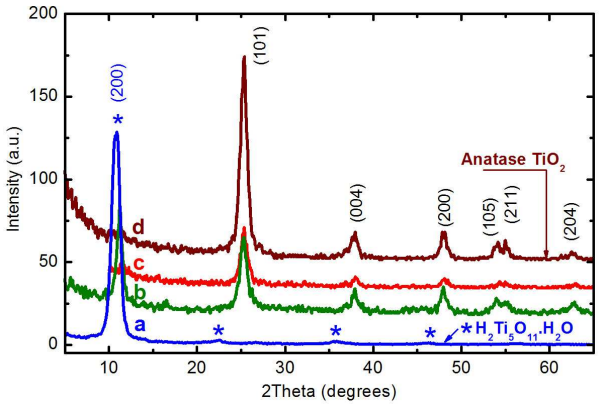

Fig. 1. XRD patterns of the TiO_2 samples after different stages of hydrothermal process: a) the first stage; the second stage at b) 110 °C, c) 120 °C and d) 130 °C for 15 h.

To find out the effect of Cr^{3+} dopant concentration on the structural properties of the synthesized samples, the XRD patterns of the $Ti_{1-x}Cr_xO_2$ samples with different molar fractions x are measured and shown in Fig. 2. It is clearly seen from the figure that all the samples synthesized with different molar fractions x exhibit pure anatase TiO_2 phase. No characteristic peaks of impurity phase have been observed. The lattice constants of samples calculated from the XRD patterns are shown in Table 1. The lattice parameters remain no change, independent on the molar fractions.

Table 1. The lattice constants of the $Ti_{1-x}Cr_xO_2$ samples with different molar fraction x

x	d_{101}(Å)	d_{004}(Å)	d_{200}(Å)	d_{204}(Å)	$a = b$ (Å)	c (Å)
0.005	3.512	2.376	1.891	1.478	3.780 ± 0.002	9.49 ± 0.01
0.01	3.514	2.375	1.892	1.478	3.783 ± 0.002	9.49 ± 0.01
0.04	3.515	2.372	1.893	1.483	3.787 ± 0.004	9.51 ± 0.03
0.10	3.501	2.369	1.897	1.482	3.78 ± 0.02	9.45 ± 0.12

The EDX spectra of samples synthesized with x = 0.005 and x = 0.1 are presented in Fig. 3. The results show that the sample with x = 0.005 was only composed of Ti and O elements, Cr

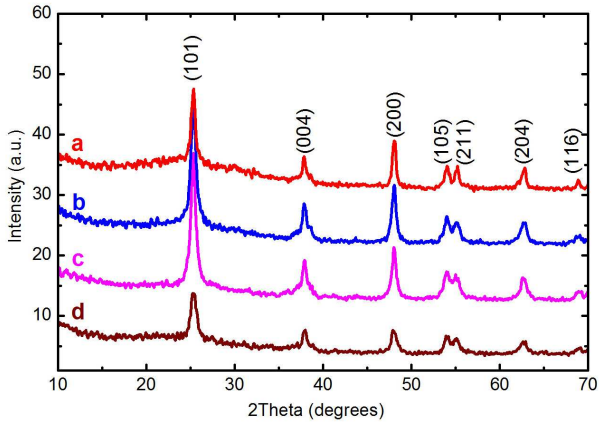

Fig. 2. XRD patterns of the $Ti_{1-x}Cr_xO_2$ samples with different molar fractions x: a) x = 0.005, b) x = 0.01, c) x = 0.04 and d) x = 0.1.

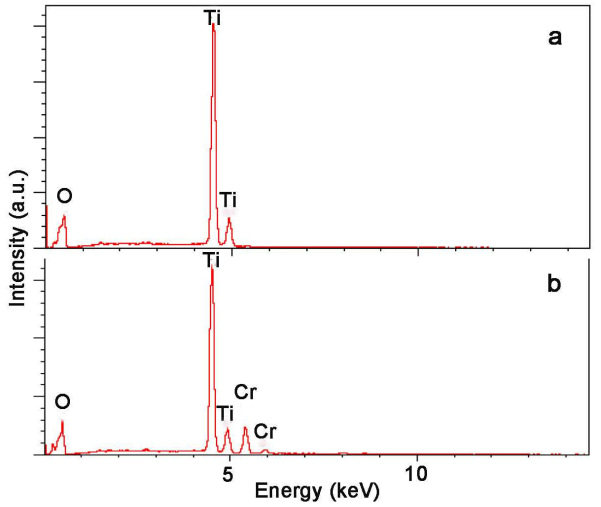

Fig. 3. The EDX spectra of the $Ti_{1-x}Cr_xO_2$ with molar fraction a) x = 0.005 and b) x = 0.10.

element was not detected due to a relatively low doping concentration (Fig. 3a). However, for the sample with x = 0.1, Cr element has been detected (Fig. 3b).

For studying the effect of Cr impurity concentration on the morphology, the SEM images of the samples synthesized with different molar fractions x were taken. The results presented in Fig. 4 show that the morphology of the samples synthesized with $x \leq 0.04$ is nanowires (see Fig. 4a,b). But, when doped with x = 0.08, beside the nanowires, small particle clusters also appear as can be seen in Fig. 4c. The amount and size of particle clusters increase with increasing x up to 0.1 (Fig. 4d).

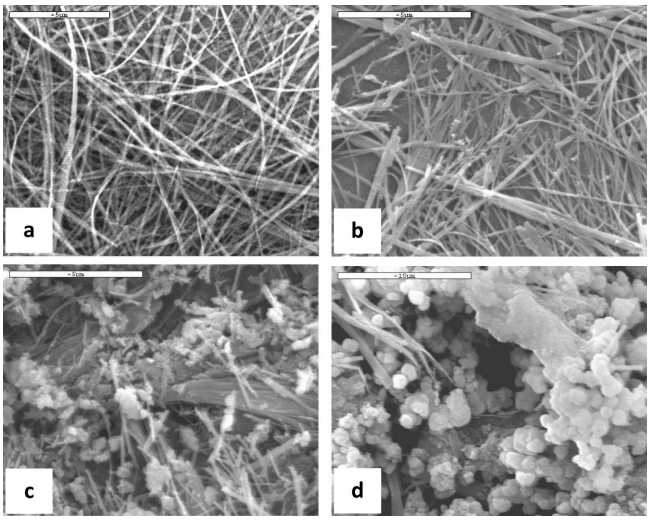

Fig. 4. SEM images of the $Ti_{1-x}Cr_xO_2$ samples with different molar fractions x, after the hydrothermal second stage: a) x = 0, b) x = 0.04, c) x = 0.08 and d) x = 0.1.

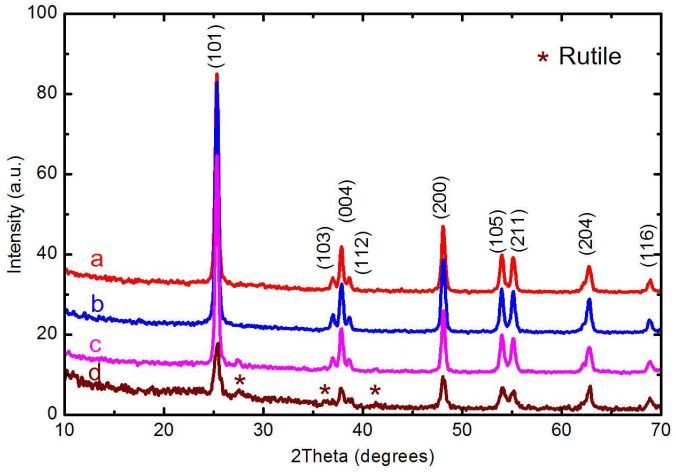

Fig. 5. XRD patterns of the $Ti_{1-x}Cr_xO_2$ samples with different molar fractions x, heat-treated at 600 °C for 3 h: a) x = 0.005, b) x = 0.01, c) x = 0.04 and d) x = 0.1.

Crystal structure of the samples is still markedly affected by a heat-treatment. The prepared samples underwent heat-treating at 600 and 1100 °C for 3 h. The XRD patterns of samples prepared with different molar fractions x and heat-treated at 600 °C for 3 h are presented in Fig. 5. As seen from the figure, for the samples with $x < 0.04$, the intensity of the characteristic diffraction peaks of anatase TiO_2 phase becomes stronger. In particular, several additional diffraction peaks of anatase phase such as (103) and (112) peaks are clearly observed as well. This proves that the heat-treated samples exhibit better crystallinity. However, for the samples with x = 0.04 and x = 0.1, beside the diffraction peaks of the anatase phase, some weak peaks of the rutile TiO_2 phase

are also observed. The lattice constants of samples are shown in Table 2. It is noted that the lattice parameters keep almost constant, being similar to the case of the samples without heat-treatment.

Table 2. The lattice constants of the $Ti_{1-x}Cr_xO_2$ samples with different molar fraction x, heat-treated at 600 °C for 3 h.

x	d_{101}(Å)	d_{004}(Å)	d_{200}(Å)	d_{105}(Å)	$a = b$ (Å)	c (Å)
0.005	3.515	2.375	1.892	1.698	3.783 ± 0.001	9.500 ± 0.001
0.01	3.515	2.375	1.891	1.698	3.783 ± 0.001	9.503 ± 0.009
0.04	3.514	2.376	1.891	1.697	3.778 ± 0.003	9.504 ± 0.005
0.10	3.507	2.378	1.892	1.696	3.77 ± 0.01	9.47 ± 0.05

Fig. 6 shows the XRD patterns of the samples with different molar fractions x, heat-treated at 1100 °C for 3 h. As seen from the XRD patterns, all the samples exhibit pure rutile TiO_2 phase. The lattice constants of samples are shown in Table 3. The results in Tables 1, 2 and 3 showed that the low Cr^{3+} dopant concentrations did not affect on the lattice constants of both the rutile and anatase crystalline phases. This is because the effective ionic radius of Cr^{3+} ion (0.615 Å) and Ti^{3+} ion (0.605 Å) in octahedral field is slightly different, that the lattice constants of both the rutile and anatase TiO_2 host crystallites are not changed in the case of Cr^{3+} concentrations lower than 10%. In particular, no other crystalline phase involving chromium oxides can be observed from all the XRD patterns. Hence, one can conclude that chromium ions have incorporated into the lattice of TiO_2.

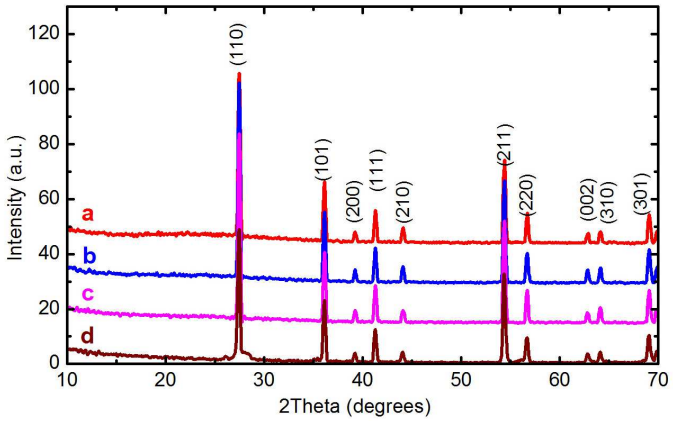

Fig. 6. XRD patterns of the $Ti_{1-x}Cr_xO_2$ samples with different molar fractions x, heat-treated at 1100 °C for 3 h: a) x = 0.005, b) x = 0.01, c) x = 0.04 and d) x = 0.1.

It is well known that Raman scattering is one of the most effective tools to research the crystallinity and defects in the materials. Fig. 7 shows the Raman spectra of the anatase $Ti_{1-x}Cr_xO_2$ samples with different molar fractions x and heat-treated at 600 °C for 3 h. The results show that Raman spectrum of Cr^{3+}-doped sample with low concentrations x = 0.005 is quite similar to that

Table 3. The lattice constants of the $Ti_{1-x}Cr_xO_2$ samples with different molar fraction x, heat-treated at 1100 °C for 3 h.

x	d_{110}(Å)	d_{101}(Å)	d_{111}(Å)	d_{211}(Å)	$a = b$ (Å)	c (Å)
0.005	3.244	2.485	2.185	1.686	4.588 ± 0.001	2.955 ± 0.001
0.01	3.245	2.486	2.186	1.685	4.59 ± 0.02	2.96 ± 0.02
0.04	3.254	2.486	2.186	1.686	4.595 ± 0.006	2.954 ± 0.005
0.10	3.246	2.486	2.185	1.686	4.588 ± 0.002	2.956 ± 0.002

of undoped anatase TiO_2 phase. In the Raman spectrum, the five allowed modes appear at 141 cm^{-1} (E_g), 194 cm^{-1} (E_g), 395 cm^{-1} (B_{1g}), 514 cm^{-1} (A_{1g}) and 636 cm^{-1} (E_g), of which mode at 141 cm^{-1} is strongest. These frequencies are 3 cm^{-1} smaller than those in anatase bulk single crystal [3, 8]. The observed shifts of Raman peaks can be interpreted as a result of the phonon confinement effect [9, 10]. When the Cr^{3+} dopant concentration increases to x = 0.01, the Raman spectrum exhibits a new series of peaks at 120, 236, 250, 292, 362, 430, 467 and 550 cm^{-1}. These new peaks become stronger in Raman spectrum of the sample with x = 0.08 and cannot be assigned to the CrO_2, Cr_2O_3, Cr_2O_5 and Cr_8O_{21} phases, because the chromium oxide phases exhibit Raman frequencies completely different from the above-mentioned new peaks [11]. Thus, the new peaks at 120, 236, 250, 292, 362, 430, 467 and 550 cm^{-1} appeared in the Raman spectra of $Ti_{1-x}Cr_xO_2$ samples with x = 0.01 and 0.08 may be related to local vibrational modes of Cr^{3+} ions located in the anatase TiO_2 host lattice.

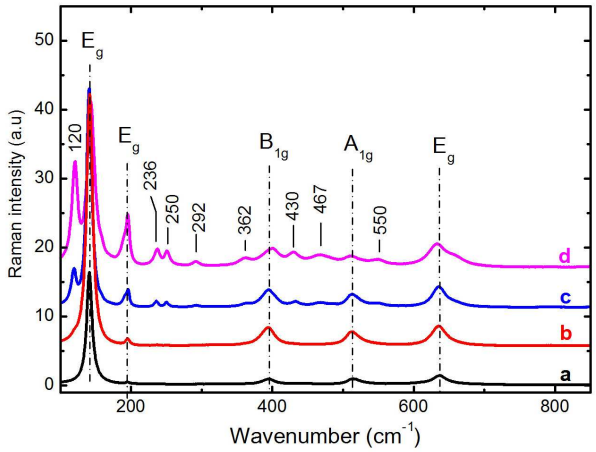

Fig. 7. Raman spectra of the anatase $Ti_{1-x}Cr_xO_2$ samples with different molar fractions x, heat-treated at 600 °C for 3 h: a) x = 0, b) x = 0.005, c) x = 0.01 and d) x = 0.08.

As mentioned above, all the samples heat-treated at 1100 °C for 3 h are pure rutile TiO_2 phase. The Raman spectra of the rutile $Ti_{1-x}Cr_xO_2$ samples with different molar fractions x are shown in Fig. 8. The positions of Raman modes of these samples are given in Table 4. It has been well known, the rutile TiO_2 has 15 fundamental modes belong to the following irreducible

representations: $A_{1g} + A_{2g} + A_{2u} + B_{1g} + B_{2g} + 2B_{1u} + E_g + 3E_u$. Among them four modes ($A_{1g} + B_{1g} + B_{2g} + E_g$) are Raman active and other four modes ($A_{2g} + 3E_u$) are infrared active. The other three modes ($A_{2g}+ 2B_{1u}$) are neither Raman active nor infrared active [12]. The Raman-active modes comprise motions of anions with respect to stationary central cations, either perpendicular to the c axis (modes B_{1g}, A_{1g}, and B_{2g}), or along the c axis (mode E_g). At room temperature, three Raman modes at 141 cm^{-1}, 444 cm^{-1} and 607 cm^{-1} are assigned to B_{1g}, E_g and A_{1g} modes, respectively, that are in good agreement with Refs. [12, 13].

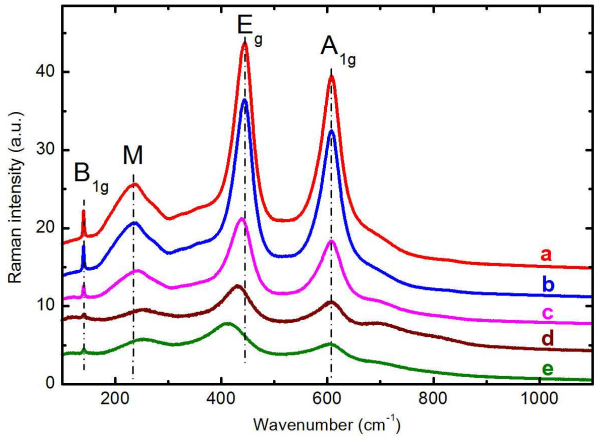

Fig. 8. Raman spectra of the rutile $Ti_{1-x}Cr_xO_2$ samples with different molar fractions x, heat-treated at 1100 °C for 3 h: a) x = 0, b) x = 0.005, c) x = 0.01 and d) x = 0.08.

Table 4. The positions of Raman modes of the rutile $Ti_{1-x}Cr_xO_2$ samples with different molar fraction x, heat-treated at 1100 °C for 3 h.

x	B_{1g} (cm^{-1})	M (cm^{-1})	E_g (cm^{-1})	A_{1g} (cm^{-1})
0.005	141	234	444	607
0.01	141	234	444	607
0.04	141	242	438	607
0.08	141	250	432	607
0.10	141	254	411	607

As for Raman peak at 234 cm^{-1}, we found that the origin of this peak is still a mystery and is temporarily denoted as M. There are several explanations for the origin of M Raman peak. It was considered as a fundamental mode, combination band, lattice disorder induced band, second-order band [12] or a mixed phonon process [13].

It is interesting to compare the peak positions and intensities of the five Raman spectra shown in Fig. 8 and in Table 4. It is clear that the positions of Raman modes B_{1g} and A_{1g} almost keep constant, not depending on the molar fractions. On the contrary, the E_g mode shifts and asymmetrically broadens towards lower wavenumber, while the M mode shifts towards higher

wavenumber as the molar fraction x increases. In addition, the intensity of all the four Raman peak is decreased with increasing the molar fraction x. It is worth mentioning that in recent work [15] the same shifting and broadening of the E_g and M modes were observed with increasing temperature from 100 K to 1100 K, and were assigned to the phonon anharmonicity.

To our knowledge, up till now, there is no general agreement about the origin of the shifting and broadening of the Raman peaks. The shifting and the broadening of the Raman modes have been related to different competing mechanisms such as phonon confinement [9, 10], non-stoichiometry due to oxygen deficiency or disorder-induced defects [14] and anharmonic effect [15].

IV. CONCLUSION

Anatase $Ti_{1-x}Cr_xO_2$ nanowires (x = 0 to 0.1) have been synthesized by two-stage hydrothermal method. The Cr^{3+} concentration and heat-treating temperature dependence of crystal structure, morphology and Raman spectra of the prepared anatase TiO_2 samples has been investigated. It is found that the samples with x = 0.005 and 0.01, heat-treated at 600 °C exhibited anatase phase, but the samples with x = 0.04 to 0.1 exhibited a mixture of anatase and rutile phases. The Raman spectra of the anatase samples with $x \geq 0.01$ exhibited a new series of peaks at 120, 236, 250, 292, 362, 430, 467 and 550 cm^{-1}, which were assigned to the localized vibrational modes related to the complexes containing Cr^{3+} ions. Whereas all the samples heat-treated at 1100 °C showed pure rutile phase, and the local vibrational modes of Cr^{3+} ions were not appeared. Instead of this, only the shifting and broadening of the E_g and M modes with increasing Cr^{3+} dopant content were observed. The lattice constants of both the rutile and anatase phases have not been affected by Cr^{3+} dopant contents.

ACKNOWLEDGMENT

This work is financially supported by VNU University of Science (Project No. TN-13-03) and Vietnam National University (Project No. QG.14.15). Authors thank the VNU project "Strengthening research and training capacity in fields of Nano Science and Technology, and Applications in Medical, Pharmaceutical, Food, Biology, Environmental protection and climate change adaptation in the direction of sustainable development" for having facilitated the equipment to complete this work.

REFERENCES

[1] M. M. B. Abbad, A. A. H. Kadhum, A. B. Mohanad, M. S. Takriff, K. Sopian, *Int. J. Electrochem. Sci.* **7** (2012) 4871.
[2] J. Zhu, Z. Deng, F. Chen, J. Zhang, H. Chen, M. Anpo, J. Huang, L. Zhang, *Applied Catalysis B: Environmental* **62** (2006) 329.
[3] H. S. Hafez, M. Saif, J. T. McLeskey, M. S. A. A. Mottaleb, I. S. Yahia, T. Story, and W. Knoff, *Int. J. Photoenergy* **2009** Article ID 240402.
[4] W. J. Yin, S. Chen, J. H. Yang, X. G. Gong, Y. Yan, and S. H. Wei, *Appl. Phys. Lett.* **96** (2010) 221901.
[5] K. B. Jaimy, S. Ghosh, S. Sankar, K. G. K. Warrier, *Materials Research Bulletin* **46** (2011) 914.
[6] A. Trenczek-Zajac, M. Radecka, M. Jasinski, K. A. Michalow, M. Rekas, E. Kusior, K. Zakrzewska, A. Heel, T. Graule, K. Kowalski, *J. Power Sources* **194** (2009) 104.
[7] H. G. Yang, H. C. Zeng, *J. Am. Chem. Soc.* **127** (2005) 270..
[8] T. Ohsaka, E. Izumi, Y. Fujiki, *J. Raman Spectrosc.* **7** (1978) 321.

[9] C. Y. Xu, P. X. Zhang and L. Yan, *J. Raman Spectrosc.* , **32** (1980) 862.
[10] H. C. Choi, Y. M. Jung, S. B. Kim, *Vibrational Spectroscopy* **35** (2005) 33.
[11] O. Monnereau, L. Tortet, C. E. A. Grigorescu, D. Savastru, C. R. Iordanescu, F. Guinneton, R. Notonier, A. Tonetto, T. Zhang, I. N. Mihailescu, D. Stanoi, H. J. Trodahl, *J. Optoelectr. Adv. Mater.* **12** (2010) 1752.
[12] T. Bezrodna, T. Gavrilko, G. Puchkovska, V. Shimanovska, J. Baran, M. Marchewwka, *J. Molecular Structure* **614** (2002) 315.
[13] G. D. Bromiley, A. A. Shirya, *Phys. Chem. Minerals* **33** (2006) 426.
[14] B. Santara, B. Pal, and P. K. Giri, *J. Appl. Phys.* **110** (2011) 114322.
[15] T. Lan, X. Tang, and B. Fultz, *Phys. Rev. B* **85** (2012) 094305.